Automation in Construction 125 (2021) 103614

Contents lists available at ScienceDirect

Automation in Construction

journal homepage: www.elsevier.com/locate/autcon

Design and fabrication of a reusable kit of parts for diverse structures

Jan Brütting [a,*], Gennaro Senatore [b], Corentin Fivet [a]

[a] Structural Xploration Lab, Swiss Federal Institute of Technology (EPFL), Passage du Cardinal 13b, 1700 Fribourg, Switzerland
[b] Applied Computing and Mechanics Laboratory, Swiss Federal Institute of Technology (EPFL), Station 18, 1015 Lausanne, Switzerland

ARTICLE INFO

Keywords:
Reuse
Kit of parts
Structures
Form finding
Space frames
Joints
Digital fabrication

ABSTRACT

Reusing structural components for multiple service cycles has potential to lower building structures environmental impact because it reduces material resource use, energy consumption, and waste production. One strategy to reuse structural components is to design structures that can be assembled, taken apart, and reassembled in new configurations. This paper presents a new computational workflow to design a bespoke kit of parts that can be employed to build structures of diverse typologies and that are not restricted to repetitive modular arrangements. Key to this method is the optimization of structural members and joints (i.e. the kit of parts) that fit multiple geometries and different structural requirements. The proposed method includes form finding and digital fabrication and it applies to the design of trusses, gridshells, and space frames. This method has been successfully applied to build three pavilion-scale prototypes from only half the number of parts compared to one-off construction.

1. Introduction

Load-bearing structures have a significant environmental impact [1–3] due to large material mass requirements as well as energy-intensive manufacturing and construction. Load-bearing structures are typically designed for a single location and use. At the end of their service, structures are usually demolished and at best material is recycled. A strategy to reduce resource use, process energy, and waste is the *reuse* of structural components [4–8]. For example, reusing reclaimed steel elements from obsolete buildings for a second service cycle avoids new steel production which reduces embodied environmental impacts by up to 56%, including additional impacts from deconstruction [7]. An alternative strategy for component reuse consists in designing a bespoke *kit of parts* whose elements are ready to be assembled in multiple structural arrangements, fulfilling different purposes. The ability to reuse kit-of-parts elements allows to manufacture only a subset of components compared to one-off constructions thus reducing material requirements. Following Howe et al. [9], the term 'kit of parts' denotes "a collection of discrete building components that are pre-engineered and designed to be assembled in a variety of ways to define a finished building". This work focuses on kits of parts for load-bearing structures.

Designing a kit of parts entails that dimensioning and detailing of all parts as well as designing the structure layouts are governed by reuse requirements. All parts have to fit the geometry of different structure layouts and all connections must allow multiple assemblies [9]. In parallel, assembly and disassembly as well as handling and shipping of all parts should be considered [9]. Example applications of this strategy have been carried out to design temporary structures including deployable structures and modular space-frame systems [10–12]. However, one drawback of modular systems is that they are often limited to repetitive arrangements.

This paper presents a new computational workflow to design a kit of parts comprising linear bars and spherical joints that can be used to build a set of diverse reticular structures, e.g. trusses, gridshells, and space frames, whose geometries are not restricted to repetitive modular arrangements.

The method has been applied to the design of a kit of parts to build the three space frame structures shown in Fig. 1. The kit-of-parts bars are tubular elements that are connected by spherical joints through bolts. The initial geometry and topology of the structures are given as input. The method comprises two steps. In the first step, the structure geometries and the kit-of-parts bars (length and cross-section dimensions) are optimized to enable the reuse of identical bars in multiple structures. In the second step, the spherical joints connection detailing (hole pattern) is optimized to reuse each joint in multiple structures.

This paper is organized as follows. A literature survey is given in Section 2. The method workflow is presented in Section 3. Section 4 describes the design and robotic manufacturing of three pavilion-scale

* Corresponding author.
E-mail address: jan.bruetting@epfl.ch (J. Brütting).

https://doi.org/10.1016/j.autcon.2021.103614
Received 30 June 2020; Received in revised form 21 December 2020; Accepted 3 February 2021
Available online 4 March 2021

prototypes. These prototypes serve as a case study to test the applicability of the proposed method to real structures and to show potential for application to existing construction systems. Discussion of results and conclusions are given in Sections 5 and 6, respectively.

2. Literature review

This study relates to three fields of research: reversible and modular construction systems (Section 2.1), architectural geometry rationalization (Section 2.2), and structural optimization for reuse (Section 2.3). Research gaps and limitations of existing methods that support the motivation for this work are given in Section 2.4.

2.1. Reversible and modular construction systems

"Design for disassembly" denotes the design of structures comprising reversible connections to allow for a non-destructive deconstruction, which enables component reuse and reduces demolition waste [13]. When design for disassembly takes into account not only deconstruction but also suitable reconfiguration scenarios, components reuse potential is the highest [10]. Following this approach, Alegria Mira et al. [11] presented a deployable scissor arch that can be used as an emergency shelter. After an initial use as a temporary structure, the arch can be disassembled to reuse its components for permanent constructions [11]. Similarly, De Temmerman et al. [14] proposed a variety of deployable structures that can be built from a common set of universal scissor components that are joined in different configurations. These examples show that deployable structures made of universal components may be a viable option for component reuse among different structures. However, deployability requirements restrict the design freedom and applicability of such structures which require specific pivot connections.

Similarly, modular structures are a viable option for temporary construction and component reuse. A well-known system comprising tubular bars and spherical joints for modular space frames is made by MERO [12]. Custom fittings and bolts enable the reversible connection of all parts and their reuse in different structural configurations [12]. A drawback of this system, however, is the restriction to certain module geometries such as platonic solids (e.g. tetrahedra and octahedra) [12]. With the availability of digital design and fabrication tools, systems like MERO or LANIK [15] have been developed further to enable the construction of freeform structures [16]. However, when used for freeform structures, most of the parts are usually customized for a single use which reduces the potential for reuse.

Rochas [17] presented a universal joint that increases design freedom for space frames: within a limited angle range, attached bars can slide on a spherical surface pivoting around the joint center so to fit different geometrical configurations. A similar joint made of an array of ball-and-socket connections was presented in [18]. Since such joints are suitable for different connection configurations, they could be reused among different structures. However, the joint systems shown in [17,18] are complex because they are made of moving parts and reconfiguration is only possible within restricted angle ranges.

De Oliveira et al. [19] presented a construction system that is based on linear bars, standard 'hubs', and custom interconnecting parts. The interconnecting parts compensate for deviations between bar directions and standard socket locations in the hubs. According to [19], this design enables the reuse of hubs while interconnecting parts must be custom manufactured to fit different structure geometries.

Brescia et al. [20] presented a reusable modular system for steel truss structures comprising linear bars and spherical joints that can be reused to build multiple structures with the objective to reduce environmental impacts. They suggested developing a computational tool to design structures that are made of components that have been reclaimed from other structures built with their proposed system. However, no detailed method formulation was given in [20]. In addition, the case studies shown in [20] feature application-specific and unique parts that might be difficult to reuse.

The review of previous work has shown that different construction systems for space frames and gridshells exist. However, most existing systems comprise repetitive modular geometries and joints are restricted to specific connection angles thus limiting the application range of such systems. In addition, to enable reuse of parts among multiple non-modular structures has received little attention.

2.2. Architectural geometry and rationalization

The field of *architectural geometry* [21] has been concerned with method development to design and analyze complex freeform surfaces and related support structures (e.g. buildings, roofs, facades). The process of making such complex designs affordable and feasible for fabrication is often referred to as architectural geometry *rationalization* [22]. A common strategy is to rationalize the geometry such that it consists of groups of identical elements that are manufactured in batches, which reduces fabrication costs. Following this motivation, Lobel [23,24] developed assembly rules to construct a large variety of polyhedral surfaces from identical equilateral triangles. Similarly, methods to panelize freeform surfaces with identical equilateral triangles or with clusters of different triangles and quads were presented in [25–28]. In

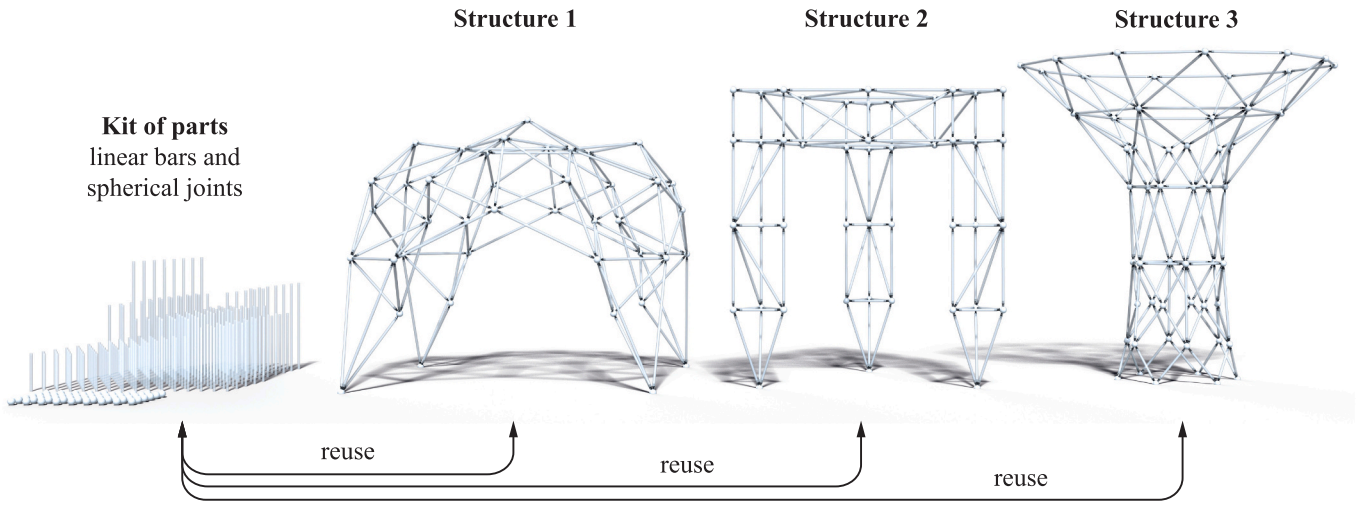

Fig. 1. Three structures that can be built from a kit of parts consisting of linear bars and spherical joints. Kit-of-parts bars and joints are reused among structures for multiple service cycles.

[27,28] grouping of panels of similar shape and dimension was carried out through clustering techniques such as *k-means* clustering [29]. Placing structural members along the panel edges obtained with these methods gives clusters of members with identical lengths. Similarly, in [30] geometry optimization was carried out on a free-form gridshell to cluster elements into a predefined number of different length groups in order to reduce fabrication costs. Driven by the erection process of elastic grid shells, Frei Otto et al. [31] developed the *compass method*, which enables the generation of meshes with a repeated edge length. The output of this method is a so-called Tchebychev net [32]. In addition to different element lengths, the assembly of freeform structures may require a large number of complex and bespoke joints. A method to reduce the number of different joints required in freeform space frame structures, while taking into account fabrication tolerances, was presented in [33].

The references given in this section are part of a large body of work that offers methods to rationalize structures of complex geometry so they can be assembled from groups of identical elements. However, most existing methods do not consider the potential to reuse identical components in multiple structures. Instead, rationalizing multiple structures simultaneously would allow the reuse of groups of identical elements among structures. Although some have suggested reusing equal-length bar elements to build different polyhedral systems [23], no rigorous computational methodology has been formulated. In [34] several free-form shapes were rationalized to be built from a single kit of parts ("Zometool system") which is made of linear elements of nine different lengths connected by one universal joint with 62 prescribed connection directions. Although different structures can be assembled from this kit of parts, restriction to nine element lengths and prescribed joint angles reduces design freedom.

2.3. Structural optimization for reuse

Structural components that can be reused in multiple structures have to be able to meet the worst expected demand over all uses. An example of this approach was given in [35]. The weight of a universal scissor component (see also Section 2.1, [11,14]) was optimized to be used in four deployable domes and seven deployable barrel vaults. Similarly, Tugilimana et al. [36] presented the structural optimization of modules for rapidly erectable bridges. The method given in [36] has been employed to optimize module topology and cross-section sizing as well as placement and orientation of modules that can be reused in two bridge structures of different height and span. As pointed out in [36,37], dimensioning structural components for reuse in multiple structures might result in oversizing individual components in order to meet the worst expected demand. This in turn can result in a less efficient material utilization compared to a one-off minimum-weight solution. However, being able to reuse the same set of components for multiple structures, allows to fabricate a smaller number of parts thus reducing the overall material input [37].

2.4. Research gaps and own contribution

The literature survey has shown that methods to rationalize structures of complex geometry with the objective to reduce component variability exist and that many construction systems for spatial reticular structures are available. However, design methods and construction systems that allow reusing structural members and joints among different and non-modular structures have received little attention.

The original contribution of this paper is the formulation of a computational design and fabrication workflow to obtain a kit of parts comprising linear bars and spherical joints that can be reused in multiple non-modular structures. In previous own work, geometry and cross-section sizing optimization methods were formulated to design multiple non-modular truss structures that can be assembled from a kit of parts [37]. Geometry optimization in [37] was formulated as a non-linear programming problem, which is computationally expensive for large-scale applications. Different to [37], in this work the structure geometries and the kit-of-parts bars are optimized through a physics engine that allows form finding and constraint solving. Since such physics engine is embedded within a CAD environment, it offers a good degree of control and it allows for interaction over the geometry design process. In addition, this work includes automation of connection detailing which was not addressed in [37]. A new optimization method is formulated to fabricate spherical joints that can be reused in multiple structures.

3. Methodology

This section presents a new computational workflow to design a kit of parts for multiple reticular structures. Reticular structures (trusses and frames) are modeled as assemblies of linear *members* that are connected at *nodes*. In the following, structure *geometry* refers to the spatial position of the nodes. The term *member length* refers to the distance between its end nodes. The connectivity relation between members is referred to as *topology*.

The kit of parts comprises linear elements and spherical couplers, which are denoted as *bars* and *joints*, respectively. Bars are regarded as physical entities that are placed at structure member positions. Joints are regarded as physical entities that are placed at node positions to provide mechanical coupling between bars. Note that, within the scope of this method, joints are neither hinged nor movable.

3.1. Design process

Fig. 2 shows a flow chart of the design methodology. Inputs are the initial geometry and topology of the set of S structures to be built from the kit of parts. Outputs are the optimal structure geometries and the kit of parts.

The blue boxes in the flow-chart of Fig. 2 indicate the three main tasks of the proposed workflow: 1) simultaneous form finding of the structure geometries and optimization of kit-of-parts bar lengths, 2) cross-section sizing of the bars for minimum weight, and 3) optimization of connection details in all spherical joints to enable their reuse among the intended set of structures. This methodology has been implemented to allow for user interaction at intermediate steps in order to control the design process in terms of performance metrics of interest which also include aesthetic quality (Fig. 2). The CAD-software Rhino6 [38] with the built-in visual programming environment Grasshopper [39] have been employed as a graphical user interface.

3.2. Form finding

Form finding of $s = 1 \ldots S$ structures is carried out simultaneously through a custom implementation of the software Kangaroo Physics v. 2.42 (K2) [40]. K2 is a physics engine that can be employed to obtain an optimal position of the structure nodes subject to applied forces. Note that in this context, the elements connecting the structure nodes do not necessarily have a physical meaning, i.e. forces are not developed as a reaction to elastic deformations through stiffness. Geometry optimization is therefore referred to as *form finding* which is primarily concerned with satisfying purely geometric constraints through a process that aims to reach set *goals* [40]. For example, a goal can prescribe geometric objectives such as proximity of selected nodes to a target shape or define a target distance between selected nodes. Within K2, an iterative solver is employed to move the position of all nodes such that all goals are satisfied within a set tolerance. The solver is based on a method which combines the Dynamic Relaxation Method [41–44] and Projective Dynamics [45]. K2 has been employed in this work for geometry optimization, instead of non-linear programming as done in previous own work [37], because of its interactive features and the ability to add custom goals (objectives) that do not require a rigorous mathematical

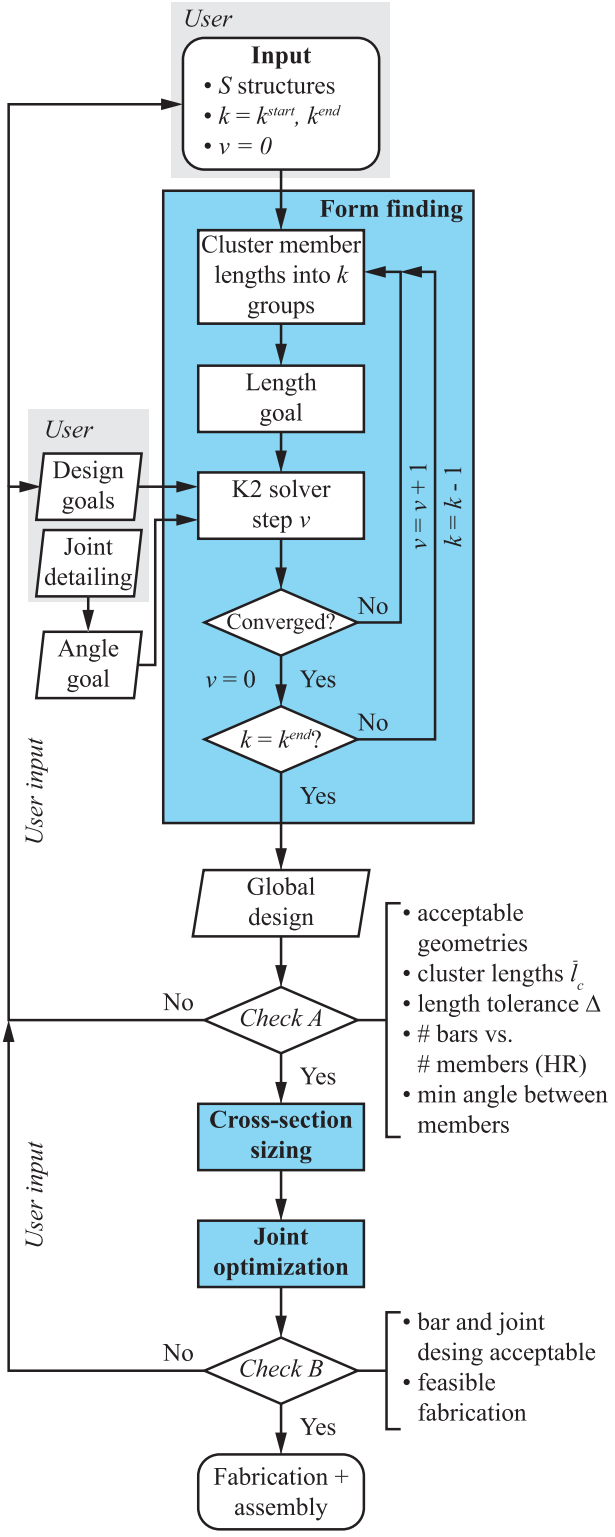

Fig. 2. Computational workflow.

formulation.

3.2.1. Clustering and length goal

To reuse kit-of-parts bars in S structures, the length of one or multiple structure members has to match with one of the bar lengths in the kit of parts, and vice versa, a bar length has to match with at least one of the member lengths. This is achieved by combining form finding with *k-means* clustering [29]. At each step v of the iterative process carried out through K2 (Fig. 2), all members of all structures are grouped into k clusters with the objective to minimize the within-cluster variance between member lengths $\boldsymbol{l}$ and mean cluster length $\bar{l}_c$ for each cluster $c = 1\ldots k$. Because member lengths are 1-dimensional data (i.e. scalar), a univariate k-means algorithm [46,47] is employed. For the special 1d case, this algorithm gives globally optimal clustering results [46].

After the optimal clustering has been obtained, a *length goal* [40,48] is defined for each member. As illustrated in Fig. 3, the goal applies a virtual 'force' F^l to the end nodes of a member such that a member length l_i will match the mean length $\bar{l}_c$ of the cluster to which member i has been assigned. For convergence, the force magnitude is proportional to the difference between l_i and $\bar{l}_c$ and thus it vanishes when $l_i = \bar{l}_c$. Note that, since $\bar{l}_c$ is the mean length of all members in a cluster, its value also changes over successive steps v.

Fig. 4 illustrates form finding and clustering through an example. Consider the layout of two structures with 18 and 15 members, respectively (Fig. 4a), and set the number of clusters to $k = 4$. First, all members are clustered into four groups by length (Fig. 4b). Next, form finding (adjustment of the node positions) is carried out with the objective to match member and cluster lengths. The optimal geometries are shown in Fig. 4(c) and the so obtained member lengths are shown in Fig. 4(d). Note that now all members in a cluster have identical lengths. Bars can be reused among both structures at member positions with same length. Therefore, the kit of parts must contain only as many bars as those that are used the most in one of the two structures (dashed regions in Fig. 4d). The number of kit-of-parts bars per cluster is denoted by n_c. Through this method, only $n^{tot} = 21$ bars are required to be able to build both structures instead of $18 + 15 = 33$ members.

Referring to the flow-chart in Fig. 2, clustering at each step v is nested within an outer loop whereby the number of clusters k is reduced by 1 at each iteration, starting from an input value k^{start} and reducing to k^{end} ($\leq k^{start}$). Setting k^{start} to a large value gives more freedom to match member and bar lengths at the beginning of the form finding process. Successively decreasing the number of clusters to k^{end} enforces member lengths to match a reduced number of available bar lengths, or in other words, it increases the number of times kit-of-parts bars are reused among the S structures.

Depending on the input structure layouts, if k^{end} is set too small, it might not be possible to match member and bar lengths exactly. In that case, bars must be produced with the length equal to that of the shortest member within a cluster to allow fitting of bars between nodes. The resulting length difference (or *gap*) between bars and end nodes is denoted with Δ. In practice, such gap could be filled with custom spacers.

3.2.2. Angle goal

Fig. 5(a) shows a spherical joint that is connected to bars via bolts. Fabrication constraints include avoidance of overlapping of bars outside

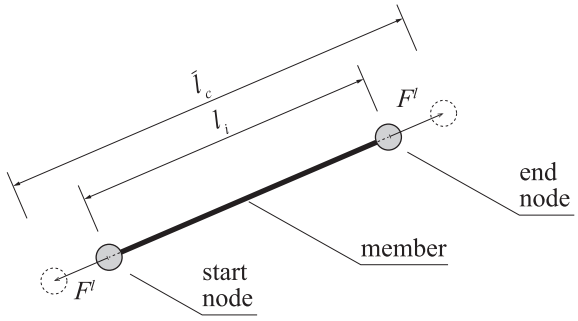

Fig. 3. 'Length goal': forces are applied at the ends of member i in order to match length l_i with cluster length $\bar{l}_c$ to which member i has been assigned.

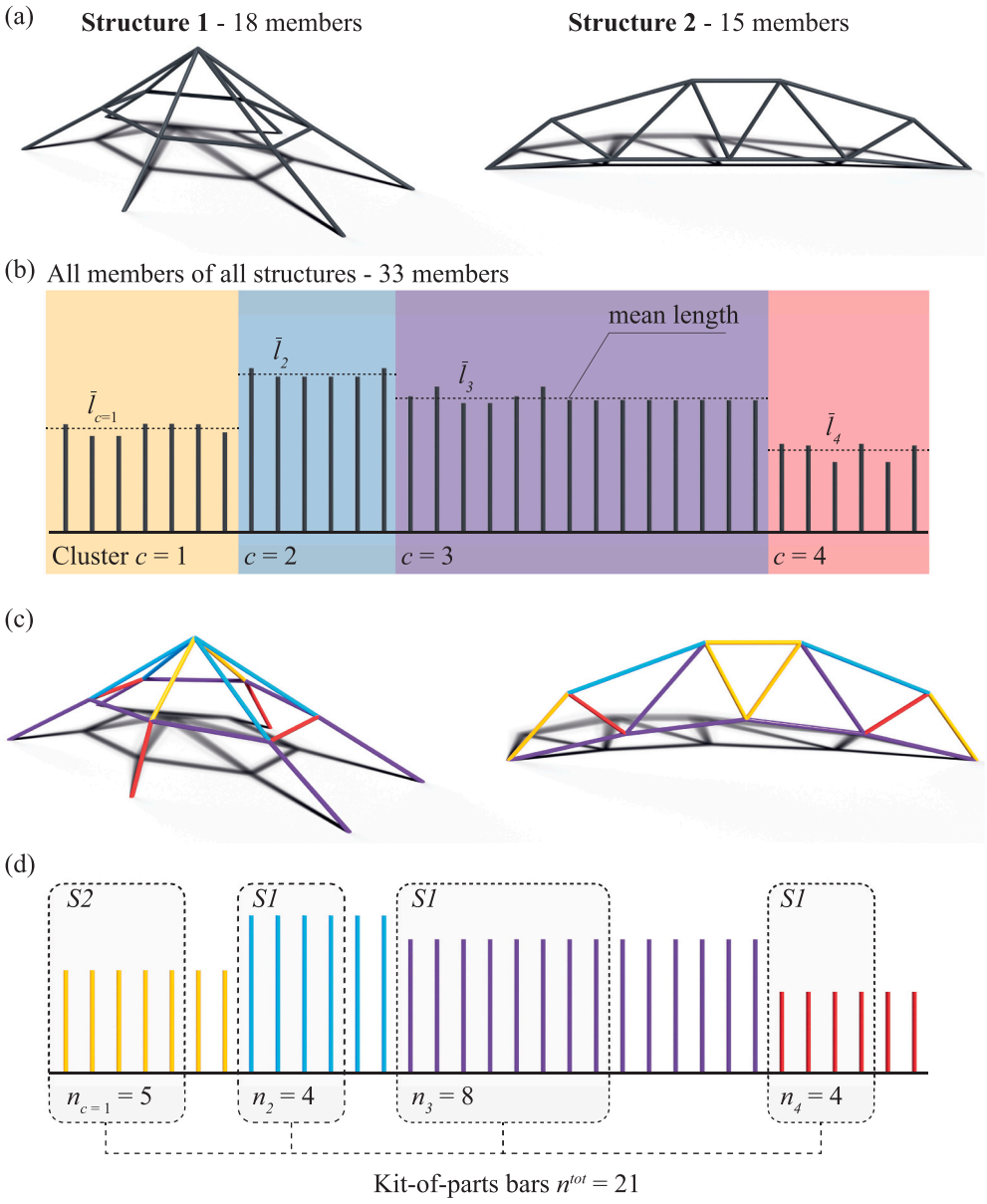

Fig. 4. Example application of the clustering and form finding method. (a) input structure layouts, (b) all members clustered into $k = 4$ groups by length, (c) optimal geometries obtained through form finding with the objective (goal) to match member and mean cluster lengths, and (d) extraction of kit-of-parts bars based on the largest number of uses in either structure Structure 1 (*S1*) or Structure 2 (*S2*). Cluster colors in (b) correspond with member colors in (c) and (d).

the sphere volume (Fig. 5a, left) and of bolt holes within the sphere volume (Fig. 5a, right). Overlapping is avoided by setting a constraint on the angle between adjacent members. Referring to Fig. 5(a), α^{in} and α^{out} indicate limit angles of members inside and outside the joint sphere volume:

$$\alpha^{in} = 2 \cdot tan^{-1}\left(\frac{W/2}{R - D}\right), \tag{1}$$

$$\alpha^{out} = 2 \cdot tan^{-1}\left(\frac{T/2}{R}\right), \tag{2}$$

where R is the joint sphere radius, T is the bar diameter, and D and W are the hole depth and width, respectively (Fig. 5(a), cf. also Sections 3.4 and 4.5). Member overlapping is avoided by ensuring that:

$$\alpha \geq \alpha^{min} = max\left(\alpha^{in}; \alpha^{out}\right), \tag{3}$$

where α is the angle between adjacent members. The angle α^{min} depends on the dimensions of the bar cross-sections, joint sphere, and bolt holes. Since bar cross-section sizing (Section 3.3) and joint optimization (Section 3.4) are carried out subsequently to form finding, an initial guess for R, T, W, and D must be set. However, cross-section sizing and joint optimization may require adapting the dimensions of bar cross-sections, joint sphere, and bolt holes. If member overlapping is no longer avoided (check A in Fig. 2), form finding should be repeated using updated dimensions. In practice, R, T, W, and D might also be constrained to available standard sizes. In addition, overlapping outside the sphere volume can be avoided through chamfering the bar ends (Fig. 5a, right).

During form finding, an *angle goal* ('ClampAngle' in K2 [40]) is defined for each pair of adjacent members (Fig. 5b): if the angle α between two members is smaller than α^{min}, a pair of virtual forces F_1^{α} and F_2^{α}

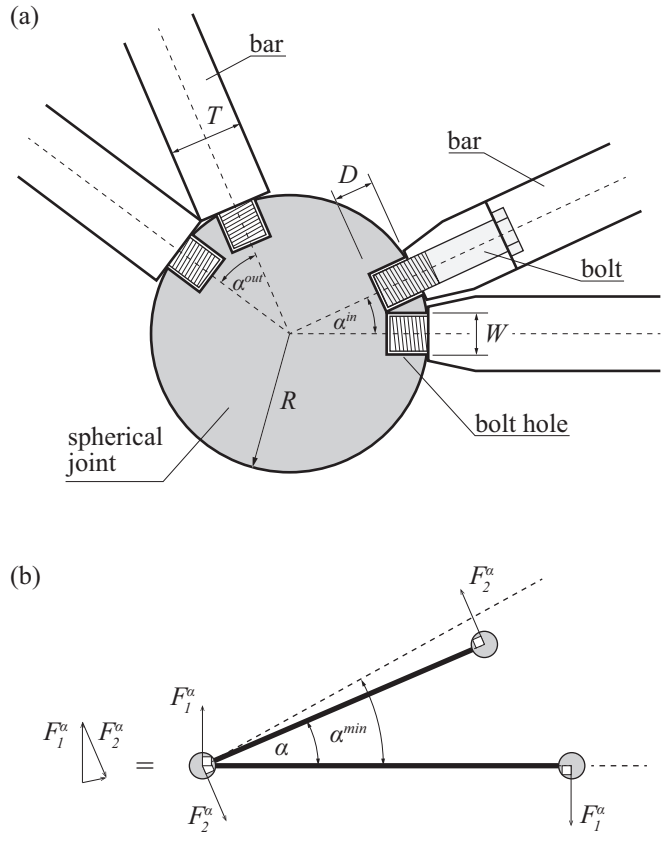

Fig. 5. Member angle constraints. (a) joint detailing and collision angles α^{in} and α^{out} between adjacent joint holes and adjacent members, (b) 'Angle goal': if angle α between two adjacent members is smaller than α_{min}, forces $F_1^\alpha$and F_2^α are applied to the member end nodes to increase angle α.

are applied to the member end nodes in order to increase α.

3.2.3. Other design goals

Kangaroo Physics (K2) allows the user to interactively control the form finding and to implement custom design goals [40,48]. For example, a goal could be to constrain selected nodes to prescribed positions or to move nodes onto target surfaces and curves. Other goals can be easily combined with the proposed length clustering (Section 3.2.1) thus offering a flexible method to design kit-of-parts structures subject to project-specific needs.

3.2.4. Form finding output

The output of the form finding process described in this section is:

- S optimized structure geometries (from S input structure geometries)
- the cluster lengths $\bar{l}_c$ for all clusters $c = 1 \ldots k$
- member clustering, i.e. which structure member belongs to which cluster
- the length difference Δ (tolerance) between member and cluster lengths
- the number n_c of bars per cluster
- the *homogenization rate* HR

The number n_c of kit-of-parts bars per cluster is also the largest number of uses of such bars among the S structures. A means to evaluate the quality of a solution obtained through this process is the *homogenization rate* HR which is defined as the ratio between the total number of members m^{tot} and the total number of kit-of-parts bars n^{tot}:

$$\mathrm{HR} = \frac{m^{tot}}{n^{tot}} \tag{4}$$

HR is bounded by the extremes $1 \leq \mathrm{HR} \leq S$. The larger HR the larger the degree of bar reuse among the S structures.

3.3. Cross-section sizing

The form finding method described in Section 3.2 produces structure geometries such that the kit-of-parts bar lengths match with specific member lengths among different structures. Next, the bar cross-sections must be sized to meet the worst expected demand when reused among structures. The simplest option is to select a single cross-section per cluster based on the worst-case loading. However, doing so might cause some bars to be highly oversized for certain member positions. Instead, better material utilization is reached when each cluster is subdivided into groups of different cross-sections. Fig. 6(a) illustrates the workflow to optimize the cross-sections of kit-of-parts bars.

A discrete cross-section optimization based on Mixed-Integer Linear Programming (MILP) is employed to obtain a preliminary subdivision of each bar length cluster into cross-section groups. Preliminary cross-section sizing optimization is carried out through an adapted version of the formulation given in [37]. Different to [37], optimal clustering and the kit-of-parts bar lengths are obtained through the form finding process described in Section 3.2. The optimization is discrete as cross-sections are selected from a standard catalog, and it is subject to stress and member buckling constraints. The structure self-weight is also accounted for. Outputs of this process are the optimal set of cross-sections per cluster as well as the assignment of members into cross-section groups. Discrete cross-section sizing optimization has been solved through the branch-and-cut method [49] that is implemented in the commercial software Gurobi [50].

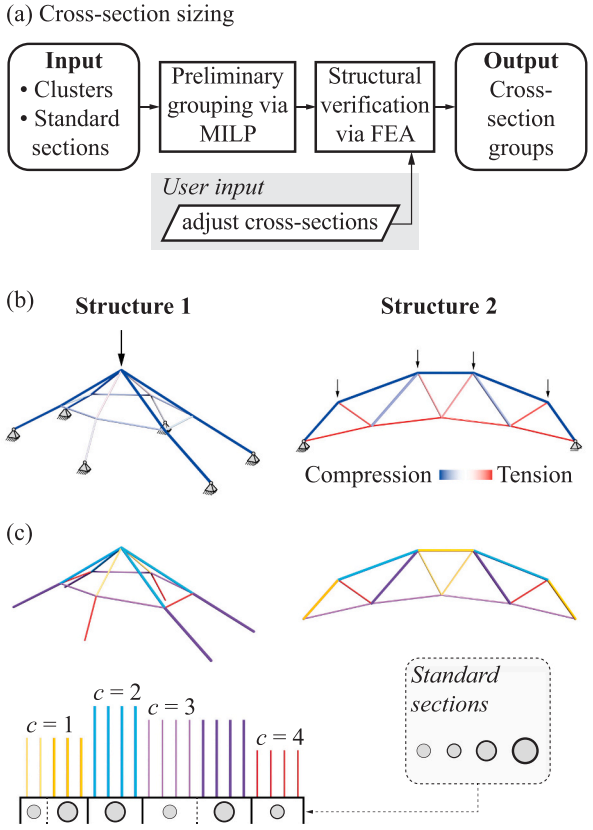

Fig. 6. Cross-section sizing. (a) cross-section sizing workflow, (b) axial forces obtained through FEA, and (c) optimal cross-section grouping.

After a preliminary cross-section sizing is obtained, a Finite Element Analysis (FEA) is carried out to analyze the structure response with regard to serviceability limit states (i.e. deflection limits) and, if required, under additional loading assumptions. In case required limits are not met, overstressed members or small stiffness members are assigned the next larger cross-section available from the standard catalog. This applies also to the whole group the sized-up members belong to. This heuristic process is repeated until all required limits are met. The final output of cross-section sizing is the number of bars to be manufactured per cross-section size. Fig. 6(b) and (c) illustrate cross-section sizing results for the example structures shown in Fig. 4. For example, the truss bottom chord members (Structure 2, right) are subjected to tension forces and hence require bars with small cross-sections. Instead, top chord members require larger cross-section bars due to member buckling constraints (Fig. 6b). Consequently, the bars used for Structure 2 bottom chord members (light purple) are also suitable for Structure 1 members that are subjected to small forces. The larger cross-section bars used for Structure 2 top chord members (cyan) can take large forces in Structure 1. Fig. 6(c) shows the optimal subdivision of the four bar length clusters in up to two cross-section size groups.

3.4. Joint optimization

Previous sections have presented the first two steps of the design method outlined in Section 3.1. Form finding (step 1) and cross-section sizing (step 2) produce kit-of-parts bars that can be reused among S different structures. This section describes the last process (step 3) of the design method whereby kit-of-parts spherical joints are optimized to be reused among S different structures.

Depending on the structure geometry and topology, members meet at a node with various orientations, which defines the *hole sets* to be drilled for coupling. In order to reuse joints among different structures, a two-step process is implemented which is illustrated in Fig. 7: 1) one node per structure is selected to be merged into one joint, and 2) the orientations of the merged hole sets (white, red and blue cylinders in Fig. 7) are optimized with the objective to obtain an even distribution of holes over the spherical surface and to avoid overlapping.

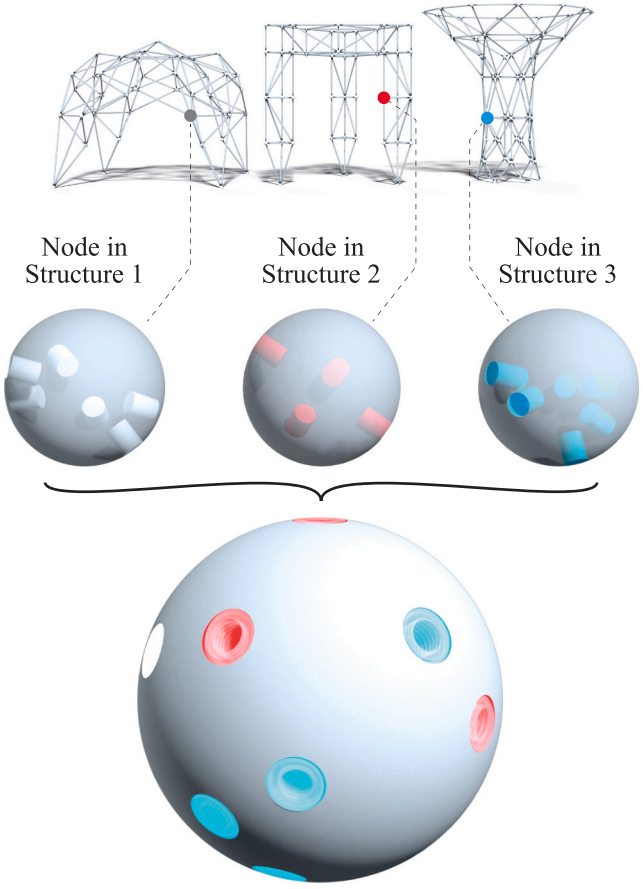

Fig. 7. Merging hole sets of multiple structure nodes into one spherical joint.

3.4.1. Selection of merged nodes

The selection of nodes to be merged into one joint is based on node *valence*, i.e. the number of members that meet at a node. A greedy heuristic is employed to merge nodes such that all joints have approximately the same sum of node valence. The nodes of each of the $s = 1 \ldots S$ structures are sorted in descending order of valence. High valence nodes in one structure are merged with low valence nodes in other structures. Note that, when the S structures differ in the total number of nodes, some joints combine less than S nodes.

3.4.2. Hole-pattern optimization

Fig. 8 shows a spherical joint (grey) of radius R and three hole sets (white, red, blue). The orientation of the holes within a set is defined through vectors that originate from the joint center. The hole voids are cylinders of diameter W and depth D (Section 3.2.2, Fig. 5). Dimensions for R, W, and D depend on joint detailing and are set prior to carrying out joint optimization (cf. Section 3.2.2). Each hole set is considered as a 'rigid body', i.e. the relation between holes (vectors) within the same set remains unchanged during optimization so that the set as a whole is reoriented. In general, the larger the radius R, the more surface is available for the distribution of holes. The objective of the hole-pattern optimization is to distribute holes evenly over the joint spherical surface in order to ensure that the distance between adjacent holes is not too small, which would otherwise reduce the joint mechanical load capacity. The main constraint is to avoid partial overlapping of holes. However, exact overlapping is allowed so that the same hole can be reused in different structures.

Optimization variables are the rotations φ_s^X, φ_s^Y, and φ_s^Z of the hole sets about the X-, Y-, and Z-axis whose origin is the center of the joint (Fig. 8). During optimization, one of the hole sets (Fig. 8, white) remains fixed because only the relation between hole sets is of relevance; hence the number of variables is 3(S-1). The volume V of the convex hull, which contains all hole centers, is employed as a quality measure for the hole distribution over the sphere surface. As an example, Fig. 9 shows

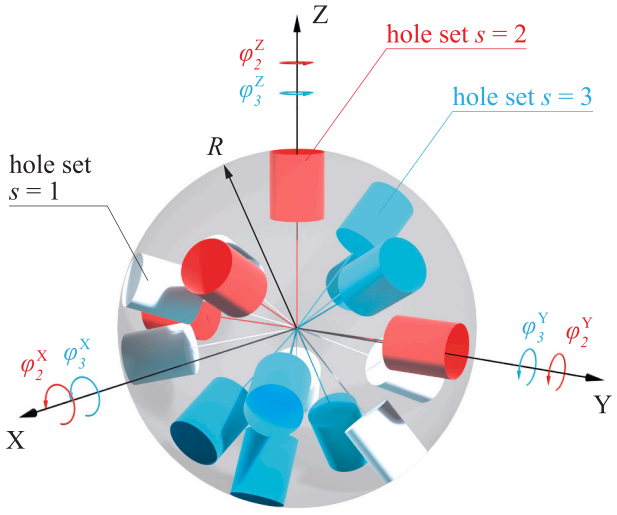

Fig. 8. Hole-pattern optimization: distribute holes evenly over the joint surface and avoid hole overlapping. The hole set in white remains fixed in position, the other two hole sets (red and blue) are rotated about the X-, Y- and Z-axis.

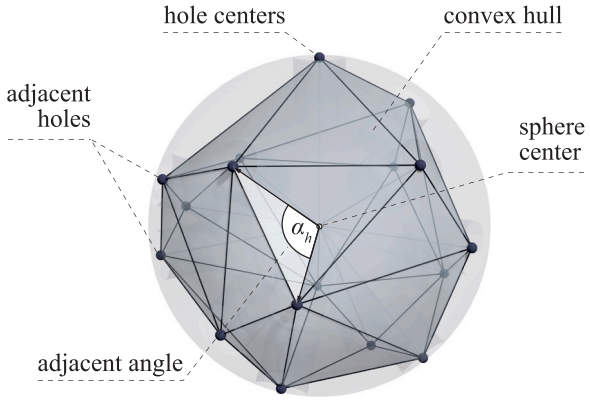

Fig. 9. Convex hull that contains all hole centers. The volume of the convex hull gives a measure of the hole distribution on the sphere surface. Angles between adjacent holes are computed from the convex hull vertices and the center.

the convex hull obtained from the hole sets represented in Fig. 8. The convex hull is a polyhedron that is enclosed by the joint sphere. In general, the larger the convex hull volume V, the better the distribution of holes.

Hole pattern optimization is formulated as an unconstrained minimization problem:

$$\min_{\boldsymbol{\varphi}} -\frac{1}{R^3}V(\boldsymbol{\varphi}) + \sum_h p(\alpha_h(\boldsymbol{\varphi})) \tag{5}$$

The objective function Eq. 5 is the sum of two terms: 1) the first term contains the volume $V(\boldsymbol{\varphi})$ of the convex hull (with negative sign to be maximized), and 2) a penalty term to steer the optimization towards feasible solutions. Since the upper bound for the convex hull volume $V(\boldsymbol{\varphi})$ is the sphere volume of $4{\cdot}\pi{\cdot}R^3/3$, the factor $1/R^3$ is employed to make the first term dimensionless. $V(\boldsymbol{\varphi})$ and the angles $\alpha_h(\boldsymbol{\varphi})$ between adjacent holes (Fig. 9) are functions of the hole-set rotations $\{\boldsymbol{\varphi} = \varphi_2^X, \varphi_2^Y, \varphi_2^Z, \ldots, \varphi_S^X, \varphi_S^Y, \varphi_S^Z\}$ which are the optimization variables. Fig. 10 shows a plot of the function $p(\alpha_h)$ that is computed for each α_h. No penalty is added when two holes overlap exactly ($\alpha_h = 0$, reuse of a hole) or when $\alpha_h \geq \alpha^{in}$ (no partial overlapping). For $0 < \alpha_h < \alpha^{in}$ the penalty function is defined as a half sine wave (Fig. 10). As described in Section 3.2.2, α^{in} denotes the limit angle to avoid overlapping of holes inside the joint sphere (Fig. 5). Overlapping of bars outside the joint sphere volume (limit angle α^{out}) is not considered because: (a) this constraint has already been enforced between adjacent members during form finding (i.e. for each hole set, cf. Section 3.2.2), and (b) such constraint is not relevant between different hole sets because structures are always assembled individually.

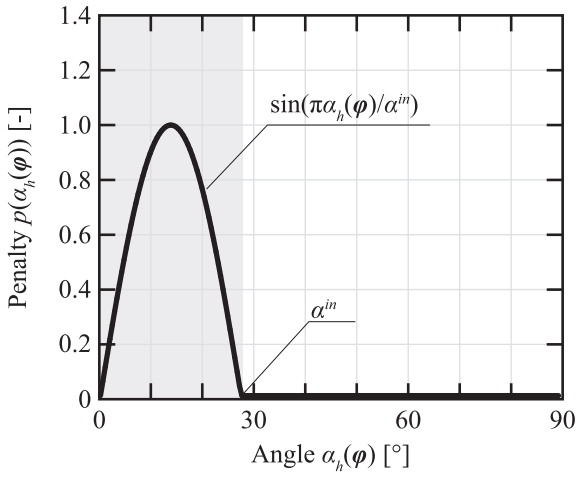

Fig. 10. Penalty function to avoid partial overlapping of holes.

If no feasible solution is obtained, it means that the selected nodes cannot be merged into a single joint and therefore separate joints must be manufactured for each node. Alternatively, another combination of merged nodes must be found.

Fig. 11 shows a surface plot of function $-V(\boldsymbol{\varphi})$ for a joint with two merged hole sets. The surface plot is obtained by computing $-V(\boldsymbol{\varphi})$ for a full enumeration of the hole set rotations $\varphi_2^X = [-180°, +180°]$ and $\varphi_2^Y = [-180°, +180°]$ which are varied with a 0.5° step. The surface plot of $-V(\boldsymbol{\varphi})$ shows multiple local minima (which represent good hole distributions) and feasible regions (no partial overlapping of holes, blue colored surface areas). The solution space is strongly non-convex and feasible regions are disconnected. These characteristics suggest the use of a global optimization method. In this work, the problem stated in Eq 5 was solved using the genetic algorithm implemented in Matlab [51]. Different from the illustrative example shown in Fig. 11, the hole-pattern optimization formulation (Eq. 5) involves three rotation axis and possibly more than two hole sets; thus a full enumeration is computationally more demanding than employing a global optimization method.

3.5. User design input

The design workflow shown in Fig. 2 (Section 3.1) involves two intermediate 'checks' to evaluate solution quality performed by the user. *Check A* evaluates structure geometries and kit-of-parts bars obtained through form finding (step 1) in terms of the metrics defined in Section 3.2.4 (e.g. n^{tot}, HR, Δ) as well as other project-specific and aesthetic criteria. *Check B* is carried out after cross-section sizing (step 2) and joint optimization (step 3) to evaluate overall performance in terms of reuse capability of kit-of-parts bars and joints. If results are not satisfactory, the following options might be taken to improve the design:

- Change of the input structure geometry or topology
- Change of cluster parameters k^{start} and k^{end} (Section 3.2.1)
- Addition or adaptation of form finding goals (Section 3.2.3)

Depending on the scale of the problem (i.e. number of total members and nodes) computation times for form finding and joint optimization are relatively small and therefore design variations can be tested

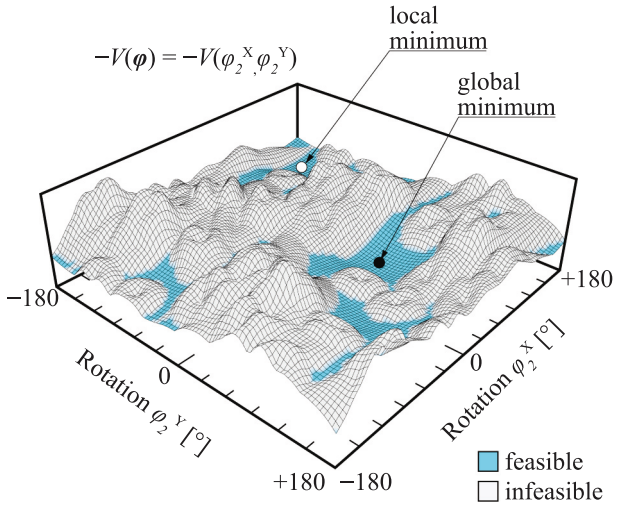

Fig. 11. Surface plot of the convex hull volume function $-V(\boldsymbol{\varphi})$ for an example joint with two hole sets. The second hole set is rotated about X- and Y-axis from −180° to +180° with a 0.5° step. Grey areas indicate infeasible regions (partial overlapping of holes), blue areas indicate feasible regions.

efficiently. Depending on the number of structure members and the size of the standard cross-section catalog, cross-section sizing optimization might require longer computation time and therefore it might not be convenient to carry out this process step at each design iteration.

4. 1-to-3 pavilion prototypes

This section presents an application of the computational workflow formulated in Section 3 to design three kit-of-parts pavilion prototypes of diverse shape and topology: a gridshell, a portal frame, and a column. The pavilion structures are shown in Fig. 12. These prototype structures were exhibited at the annual symposium of the International Association of Shell and Spatial Structures (IASS) held in Barcelona in 2019. The pavilions are named '1-to-3' in reference to the kit-of-parts design strategy. The main objective was to showcase the possibility to reuse components among three non-modular structures of very different form. Among the exhibition requirements was to limit the pavilion dimensions within a $4 \times 4 \times 4$ m volume and the total weight to 192 kg. Constraints which had a significant influence on geometry and sizing of the three structures. To obtain a light-weight and transportable kit of parts, acrylic glass tubes were selected for the bars and wooden spheres for the joints. In this context, the terms "bar" and "tube" have identical meaning and therefore will be used interchangeably. The sum of structure members and nodes in the three structures are 351 and 140, respectively. Through the application of the design process formulated in this work, the three structures are assembled with only 170 bars ($HR_{bars} = 2.06$) and 54 joints ($HR_{joints} = 2.59$). The high homogenization rates so obtained allow for significant mass savings of up to 53% compared to the case in which each structure is individually designed and optimized. Note that paneling (cladding) has not been considered.

4.1. Detailing

Fig. 13 shows an exploded-view drawing of the connection between bars and joints. The design is inspired by the MERO ball and tube system but adapted to be fully dismantlable and producible with available fabrication tools. The joint sphere radius ($R = 40$ mm) is an outcome of the design process which is given in next sections. Holes are drilled into the wooden spheres based on the pattern obtained from joint optimization. Steel threaded inserts are placed into the holes. An M8 bolt connects each tube to the wooden sphere. The use of M8 bolts determined the size of the steel threaded inserts which have a width $W = 12$ mm and a depth $D = 15$ mm. A 3d-printed hexagonal sleeve and a lid are inserted between sphere and the open tube end. Since the bolt head inside the tube is not accessible, a lock key is employed to rotate the bolt through the hexagonal sleeve.

Compression forces are transferred from bars to joints through contact of all parts. Tension forces are transferred through friction between the tube and the lid: a rubber pad expands against the inner tube wall as the bolt is tightened. The connection is fully reversible and allows multiple assembly cycles.

The mechanical capacity of the connections is adequate for the pavilion-scale application described in this paper. The structures have been designed to take small loading, which is predominantly self-weight. For larger scale structures, different materials such as steel could be employed for all parts and the lid could be reversibly attached to the tube through a threaded fitting.

4.2. Form finding results

Fig. 14(a) shows the input layouts and indicates the number of members and nodes for each structure. For this problem size, the computation time to complete a form finding task, performed on an Intel i7-6820HQ 2.70 GHz CPU, varied between 2.0 and 7.0 s. Computation time includes all iterations over the number of bar-length clusters k from k^{start} to k^{end} (Fig. 2). Since the computation time to complete form finding was relatively small, it was possible to adapt the design of each structure interactively, e.g. by fixing or freeing selected node positions and by adding 'artificial' forces to achieve specific objectives.

Fig. 14(b-d) shows three intermediate steps of the form finding process and Fig. 14(e) the final design. All configurations shown in Fig. 14(b-e) are those obtained with k^{end} clusters. Per step, bars represented with the same color have identical length and color mapping indicates correspondence between members and kit-of-parts bars.

In step b) structure member lengths are clustered by setting $k^{start} = k^{end} = 9$. This results in a kit of parts that contains 208 bars, which gives a homogenization rate (HR) of 1.69. Reducing k^{end} from 9 to 7 in step c) enforces the structure members to match fewer available bar lengths and thus the number of kit-of-parts bars reduces to 190 (HR = 1.85). In step d), upward-pointing vertical forces F^{up} are applied to Structure 1 top nodes in order to increase height clearance (Fig. 14d, left). This extra constraint improves matching between member and bar lengths, thus the number of bars is further reduced to 178 (HR = 1.97). In step e) k^{end} is set to 6 which reduces the number of bars further to 170 (HR = 2.06).

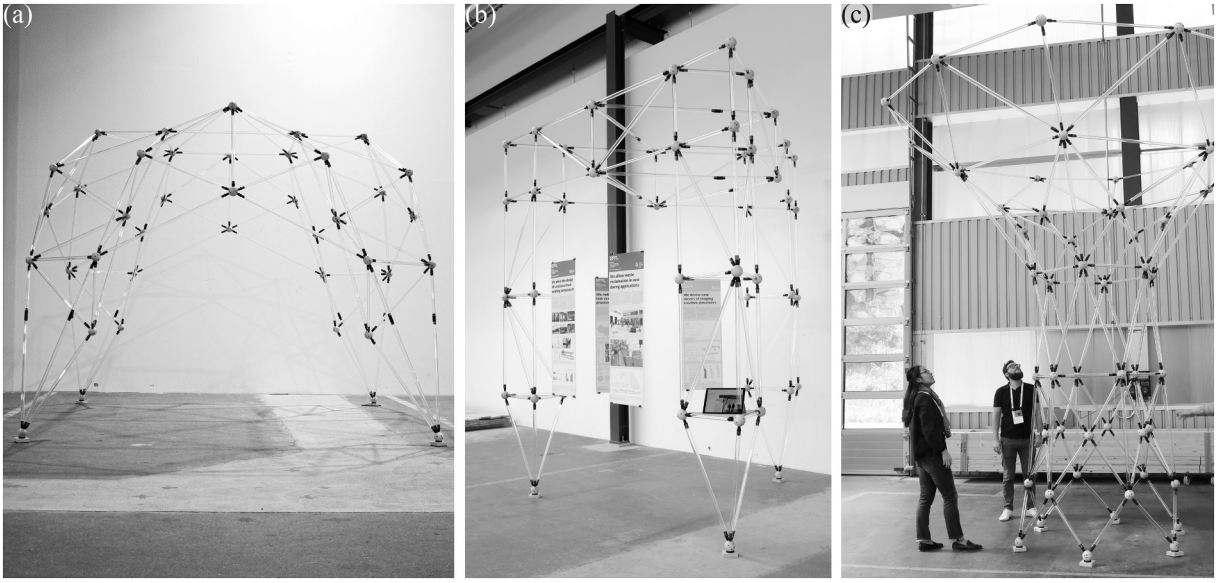

Fig. 12. 1-to-3 pavilion structures. (a) gridshell, (b) portal frame, and (c) column.

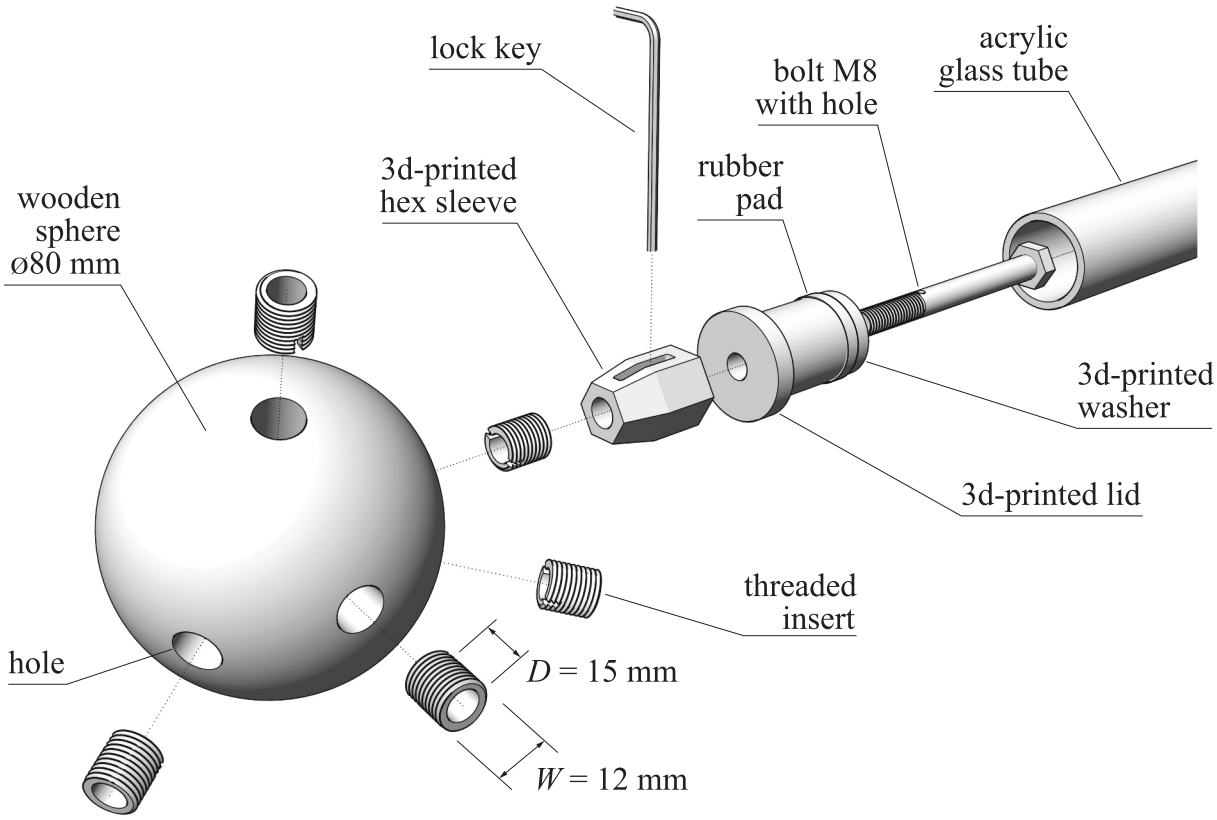

Fig. 13. Exploded-view of the connection between spherical joints and tubular bars.

The configuration in (e) was deemed as satisfactory in terms of homogenization rate as well as from an aesthetic point of view. For all three intermediate steps as well as for the final design, the difference between member and bar lengths is $\Delta < 0.1$ mm, which is negligible in terms of fabrication and assembly tolerance.

Referring to the final design (Fig. 14e), Table 1 gives the bar length $\bar{l}_c$ for each cluster, the total number of bars n_c per cluster, and the number of uses per structure for each cluster. After subtracting the joint sphere radius (40 mm) and the combined length of connecting parts (Fig. 13), the bar lengths are between 432 and 1479 mm. The kit of parts contains 170 bars (HR = 2.06) instead of 351 bars, which would be the total numbers of bars required if the structures were built individually. Note that the kit of parts contains only 38 more bars than the total number of members in Structure 3 (132).

4.3. Bar cross-section sizing

A catalog of standard circular hollow sections of size ø20/16, ø25/21, ø30/26, and ø38/32 mm (outer diameter / inner diameter) is selected based on the expected loading demand. In addition, tubular bars with such cross-section sizes can be slid into each other to reduce packaging volume. No cross-section smaller than ø20/16 is selected because the M8 bolt head, which has to fit into the tube, is 15 mm in width.

Subdivision of kit-of-parts bar clusters into groups of different cross-section sizes is obtained by applying the methods outlined in Section 3.3. Preliminary cross-section sizing is carried out through the MILP-based structural optimization. This formulation considers force equilibrium for each structure under self-weight and subject to stress as well as member buckling constraints. Geometric compatibility and nodal displacement constraints are excluded to reduce computational complexity. The weight of bars and joints is lumped to the nodes. A joint weighs approximately 1.5 kg, including bolts, threaded inserts, and 3d-printed parts (Fig. 13). A load safety factor of 2.0 is applied to account for model and assembly uncertainty. Subsequently, cross-section sizing and deflection limits are evaluated through a finite element analysis (FEA) which has been carried out in Sofistik [52]. Contrary to preliminary sizing in which the structure members are pin-jointed and thus can take only axial forces, the FEA model comprises bending-resistant elements (beams) that are rigidly connected, which gives a more accurate prediction of the structure response.

The bar chart in Fig. 15 indicates the bar length $\bar{l}_c$ and the total number of bars n_c for each cluster. Each cluster is subdivided in up to two groups of cross-section sizes. The cross-section size groups are labeled with (a) ø20/16, (b) ø25/21, and (c) ø30/26. The number of bars per cross-section group is denoted by n. For example, the 48 bars of cluster $c = 3$ (blue) are divided into 12 and 36 bars with cross-section ø20/16 and ø30/26, respectively. At the bottom of Fig. 15, cross-section subdivision is reported for both preliminary sizing through MILP and that obtained through FEA analysis. In some cases (clusters 1, 2, 4, and 5), FEA results lead to increasing the size of a cross-section group.

Fig. 16 shows cross-section sizing distribution among the three structures and kit of parts. For example, the ø20/16 bars (light blue) are assigned to the topmost members of Structure 1 and Structure 3, where they are subjected to low forces. Instead, the larger ø30/26 bars are assigned to members subjected to higher forces such as those in proximity of supports as well as in columns of Structure 2.

The total mass of the 170 kit-of-parts bars is 23.5 kg (acrylic glass tubes with a density $\rho = 1.19$ g/cm^3). Since cross-section sizing of kit-of-parts bars is based on the worst-case loading among different structures, oversizing occurs with respect to sizing carried out for each structure separately. The total number of members for the structures considered in this case study is 351. If the smallest cross-section of size ø20/16 was

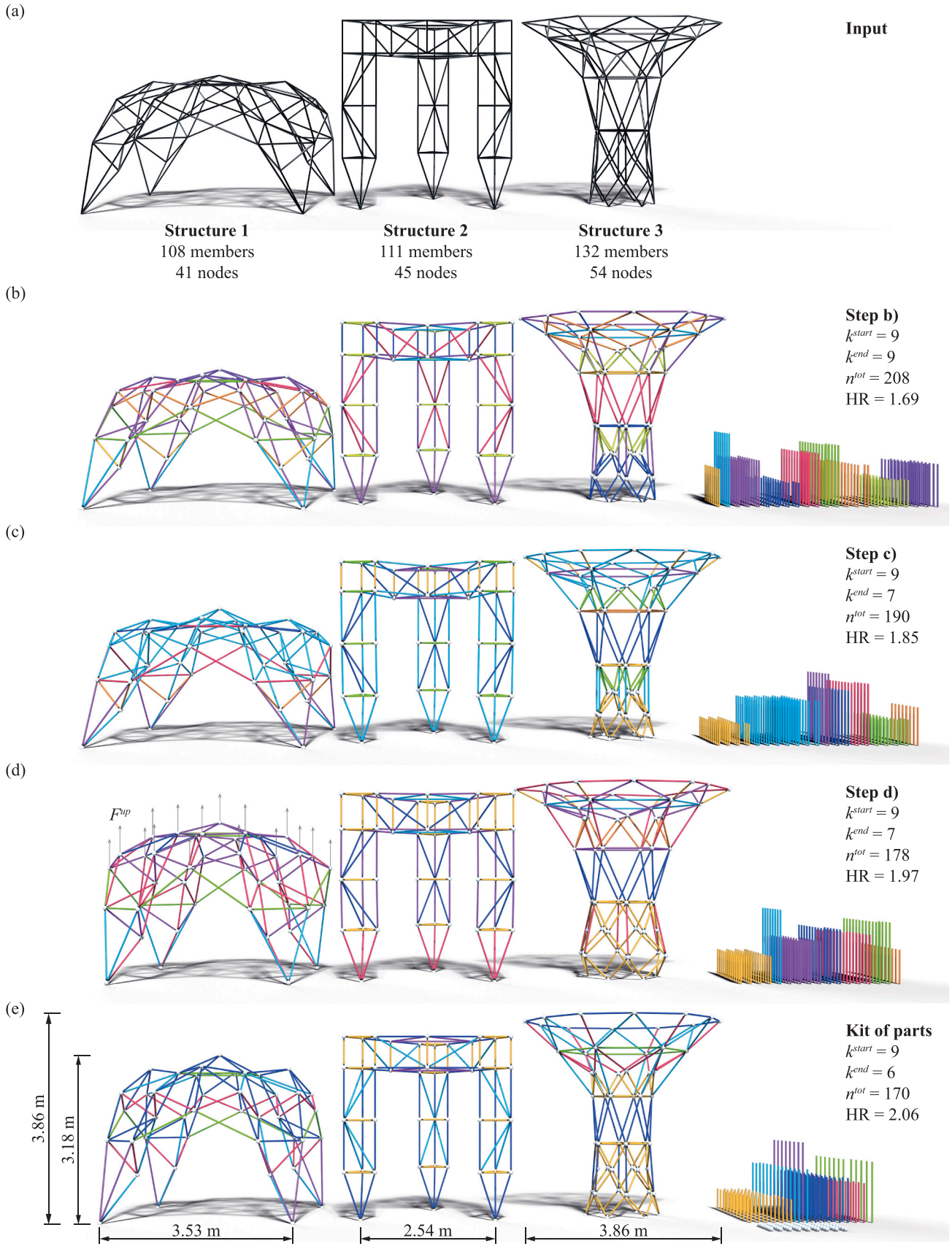

Fig. 14. Form finding process (members and bars of same color have identical lengths). (a) input structure layouts, (b, c, d) intermediate geometries and corresponding kit of parts, and (e) final design.

Table 1
Cluster length and number of uses, 1-to-3 pavilion case study.

Cluster c	1	2	3	4	5	6
Color in Fig. 14(e)	yellow	red	blue	cyan	green	purple
Length $\bar{l}_c$ [mm]	432	732	829	989	1126	1479
# of bars per cluster n_c	**60**	**24**	**48**	**18**	**12**	**8**
# of uses Structure 1	0	24	48	16	12	8
# of uses Structure 2	48	0	39	18	0	6
# of uses Structure 3	60	18	30	18	6	0

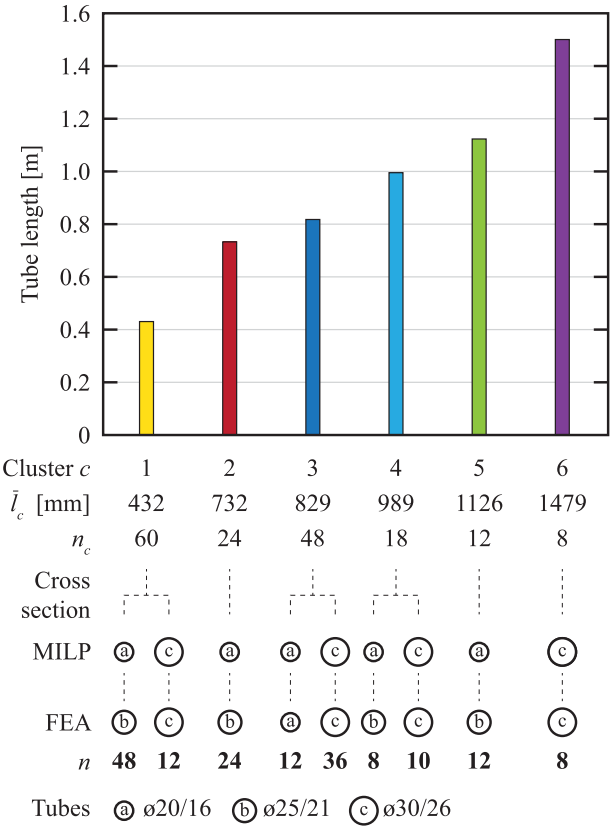

Fig. 15. Bar lengths and cross-section sizing.

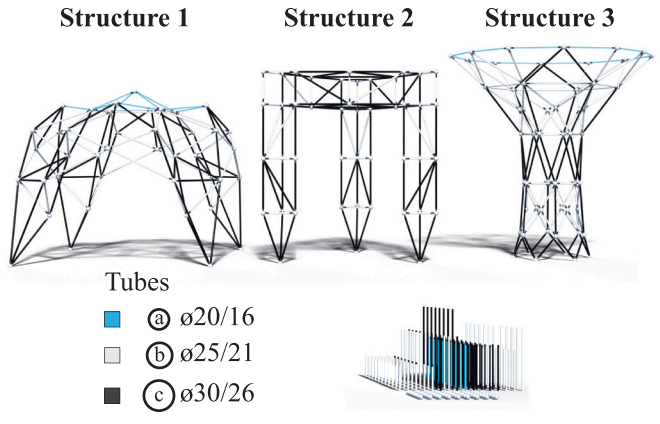

Fig. 16. Member cross-section sizes in all three structures and the kit of parts.

assigned to each of the 351 members, the combined weight would be 36.8 kg, which is a theoretical lower bound. Therefore, the ability to reuse bars among structures reduces material input mass by at least 36% compared to one-off construction.

4.4. Cutting stock optimization

The bars had to be cut to length from 2.0 m standard length acrylic glass tubes. A *cutting stock optimization* [53] has been employed to minimize trim losses (i.e. waste). Cutting stock optimization is commonly applied in industrial processes to reduce trim losses and waste for materials that are in the form of one-dimensional stocks such as steel rebars or structural steel sections [54].

Fig. 17 shows a bar chart that illustrates the optimal cutting pattern and the number of 2.0 m standard length tubes that are required to obtain the kit-of-parts bars. Color mapping indicates to which cluster each bar belongs. Cut-off waste is represented in black. An Integer Linear Programming (ILP) based cutting stock formulation [53], which gives globally optimal cutting patterns, is employed. The ILP-problem is solved through the branch-and-cut solver implemented in commercial software Gurobi [50]. The computation time to obtain the optimal patterns shown in Fig. 17 was 2.4 s. In total, 6, 31, and 32 standard length tubes with a cross-section size of ø20/16, ø25/21, ø30/26, respectively, are required to cut to length the 170 kit-of-parts bars. Cut-off waste amounts to 2.2 kg which is 9% of the total mass of the 69 standard length tubes.

Besides material reduction, being able to reuse kit-of-parts bars can also result in monetary cost savings. The total cost of 69 acrylic glass tubes with 2.0 m standard length was 1050 CHF (Swiss Francs). Instead, if the structures are designed individually and assuming all members are assigned the smallest cross-section (ø20/16), 351 members must be cut from 142 standard length tubes which would have cost 1820 CHF (lower bound).

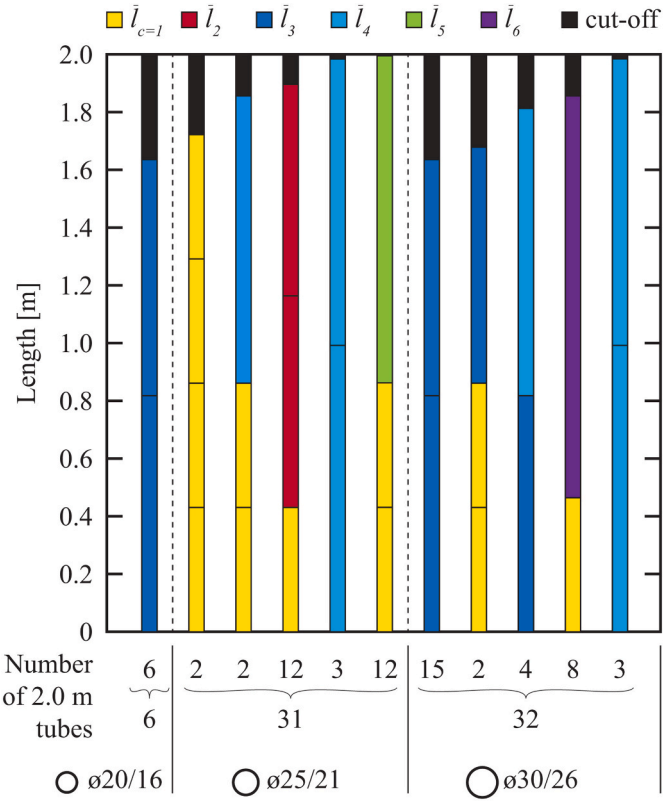

Fig. 17. Cutting stock optimization for the kit-of-parts bars cut from 2.0 m standard length tubes.

4.5. Joint optimization and manufacturing

The objective of joint optimization (Step 3 of the design process in Fig. 2 and Section 3.4) is to minimize the number of joints that are required to assemble the three pavilion structures, and consequently, to increase reuse of all joints among the structures. In the case of the three pavilion structures, there are 140 nodes. The minimum number of joints is 54, which is the number of nodes in Structure 3 (Fig. 14a). Beech-wood spheres were available from a supplier with standard radii of 35, 37.5, and 40 mm. If all joint spheres have a radius of $R = 40$ mm, it is possible to obtain a feasible solution whereby only 54 joints are required to merge the hole sets of all 140 nodes ($HR_{joints} = 2.59$). For comparison, if one joint was produced for each of the 140 nodes individually, smaller spheres with a radius of 37.5 mm could be used because fewer holes are required to fit on each joint spherical surface.

The total mass of 54 beech-wood joint spheres with 40 mm radius is 10.4 kg (material density $\rho = 0.72$ g/cm^3). The total mass of 140 joints with 37.5 mm radius is 22.3 kg. Therefore, the ability to reuse 54 joints among the three structures reduces material input mass by 53%. A similar reduction in monetary cost is obtained. The total cost of 54 wooden spheres with 40 mm radius is 265 CHF (unit price 4.90 CHF), whereas 140 spheres of 37.5 mm radius spheres would cost 588 CHF (unit price 4.20 CHF).

Considering the chosen structure geometries (Fig. 14e), a joint sphere radius smaller than 37.5 mm could not be selected because adjacent members would overlap inside the sphere (i.e. angle constraint α^{in} is not satisfied, Eq. 1, Section 3.2.2). If smaller joint spheres would be required, the form finding process should be repeated starting from a different set of input parameters for the joint sphere radius R, bar diameter T, bolt hole depth D, and width W, so to increase the angle limit α^{min}. This shows that joint detailing and form finding are tightly interrelated. Since the proposed workflow allows for user interaction, these adjustments can be easily incorporated.

The average computation time for the hole pattern optimization of a single joint is 9.6 s and a total of 8.6 min for all joints. For a preliminary assessment it might be of interest to evaluate only whether feasible solutions exist, thus neglecting holes distribution quality over the joint surface (i.e. omission of the first term in Eq. 5). In this case, joint optimization is terminated as soon as a feasible solution is obtained, which reduces the average computation time per joint to 0.2 s (a total of 11 s for all joints).

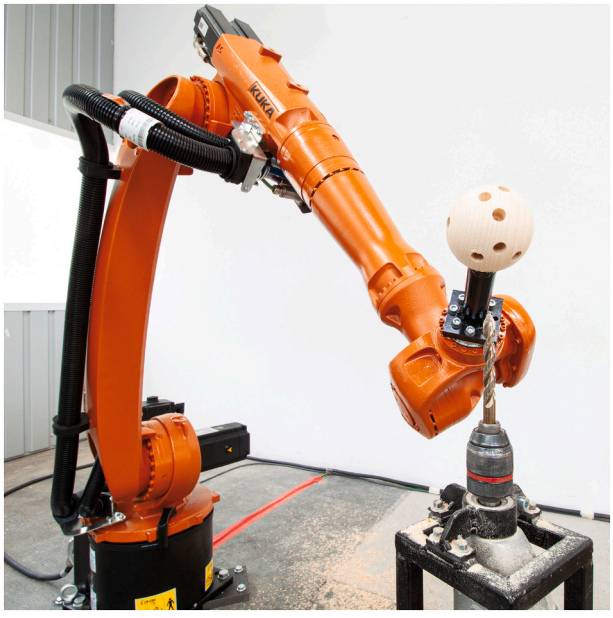

Fig. 18. Joints are fabricated with an industrial 6-axis robot and a stationary drill.

The optimal orientation of the hole sets in each joint is translated into numerical control code to drill the required holes with an industrial robotic arm. Fig. 18 shows the drilling setup: a joint sphere is attached to the robot arm via a custom mount and then it is maneuvered onto a stationary drilling machine. Depending on the fabrication setup, avoidance of collisions between robot arm and drill holder might impose additional constraints on joint angle limitations (α^{min}). In this work, this problem was not governing and hence not considered in more detail. The threaded inserts (Fig. 13) have been manually fixed into the holes.

4.6. Kit of parts and assembly

The complete kit of parts consisting of acrylic tubular bars, wooden spherical joints, 3d-printed connectors, and bolts is shown in Fig. 19(a). Since all connections between tubular bars and joints are reversible, the total number of connecting parts is reduced further. For example, instead of two bolts for each end of the 170 tubular bars, only two times 132 bolts are required in the kit of parts. This is because 132 is the largest number of members among the three structures (Structure 3, cf. Fig. 14).

Fig. 19(b) shows a joint with connected tubular bars for one of the nodes in Structure 1. For clarity, the free holes that can be seen in Fig. 19 (b) are used for the assembly of the other two structures. Small black dots located in the proximity of each hole indicate the structure the hole belongs to (index $s = 1, 2, 3$). This information, together with digital 3d-models, is employed to facilitate the manual assembly. Fig. 12 shows the three structures successively built from the kit of parts.

5. Discussion and future work

The realization of the three pavilion prototype structures has shown application potential and feasibility of the methodology formulated in this work to design reticular kit-of-parts structures. Cladding, roofing, and generally covering has not been considered in this work. Depending on the structure topology, cover panels of different shapes (e.g. triangles or quads) might be required. Since members are clustered into groups of identical length, it might also be possible to obtain cover panels that could be reused among structures. Future work could investigate panel reuse by extending the form finding technique given in this paper with the methods outlined in Section 2.2. Panel reuse will add further constraints and therefore it could have a positive or negative effect on member as well as joint homogenization rates. This pending question could be the subject of future work.

A 1-dimensional *k-means* algorithm [46,47] has been employed for member length clustering. The small computation time required by this algorithm to obtain an optimal clustering solution makes it particularly suitable for user interaction. However, *k-means* clustering requires setting a priori the number of clusters k, which is likely to produce sub-optimal solutions. Future work could investigate member length clustering through other techniques including reinforcement and unsupervised learning. Of particular interest are methods whereby the optimal number of clusters k is an output.

Form finding and cross-section sizing have been carried out separately. This allows for a fast and interactive form finding process. However, the form finding process is not subject to structural constraints (stress and deflection limits) and therefore it might produce solutions that are not structurally efficient. Future work could investigate the combination of fast clustering techniques with structural geometry and cross-section sizing optimization.

The pavilion structures were designed for an exhibition with the main objective to showcase the possibility to reuse parts among three non-modular structures of very different form. For this reason, the Finite Element Analysis (FEA) carried out for the pavilion case study has been simplified by considering a single load case (self-weight) per structure. Depending on the application and structure type, the FEA should be

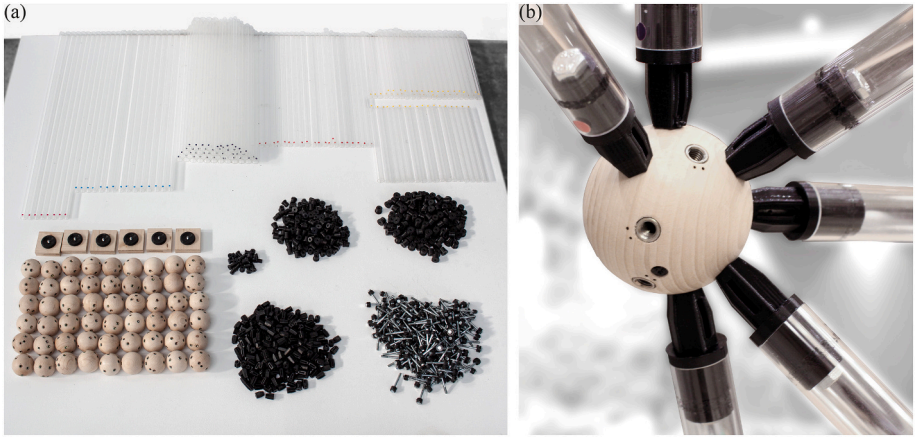

Fig. 19. Fabricated parts. (a) complete kit of parts to build the three pavilion structures: tubular bars (transparent acrylic tubes), spherical joints, 3d printed connectors, bolts, and support sockets, (b) detail of a wooden spherical joint with connected tubular bars. Free holes are used to connect members of the other two structures.

adapted to consider all relevant loading scenarios as well as non-linear effects and global stability.

The joint optimization method given in this paper, which allows using the same spherical joint for assembly of different structures, could be extended to existing construction systems that are based on spherical joints (e.g. MERO, LANIK). For triangulated double-layer systems (i.e. space trusses) whose members are primarily subjected to normal forces, the proposed connection system applies directly. For single-layer structures, the joints and centric bolts might be subjected to bending. Different bending-resistant joining systems for single-layer structures are proposed in the literature [16]. In future work, the idea of merging multiple nodes of different structures into one reusable joint could be extended to joint typologies other than spherical ones.

One limitation of the presented kit-of-parts design approach is that it requires a-priori knowledge of the set of structures and their future uses. This might limit the application of the proposed methodology to temporary structures. Future work could extend the work to large-scale structures as well as to components such as slabs and walls to widen the application range for kit-of-parts structures.

Reducing the upfront material input through kit-of-parts solutions might not necessarily mean that kit-of-parts structures have a lower life-cycle environmental impact than systems made of new material. It is expected that the possibility to reuse elements for multiple service cycles will reduce environmental impact. However, future work should verify this assumption through a Life Cycle Assessment that considers all service cycles of the kit-of-parts structures, including all intermediate processes such as assembly, maintenance, transport, and storage. In practical applications, it will also be necessary to consider component durability and wearing caused by reassembly.

6. Conclusion

This paper has presented a computational workflow to design and fabricate kit-of-parts linear bars and spherical joints that can be reused to build structures of diverse shape and topology. This paper has also introduced a new formulation to optimize connection details with the objective to reuse spherical joints among different structures.

The proposed workflow allows for user interaction and customization. Since bars and joints geometrically fit to positions in each of the intended designs, they can be reused among structures for multiple service cycles. The structures can have different uses and can be built in different locations. Through the kit-of-parts solutions obtained with the methodology formulated in this paper, material input is significantly reduced with respect to one-off design solutions because most parts can be reused. Therefore, this methodology contributes to resource use reduction and to lower structure environmental impacts. In addition, reducing the number of manufactured parts results in monetary-cost savings compared to one-off design solutions.

The workflow formulated in this work has been successfully applied to obtain a kit of parts for three pavilion-scale structures. Three structures of very different shape and topology could be built with relatively simple and established fabrication methods, which shows potential for application to real-world configurations. From a broader perspective, despite the often-attributed low-tech nature of reuse, this work has also shown how the combination of advanced computational techniques (i.e. form finding and structural optimization) with digital fabrication can contribute to a circular economy.

Funding

This research did not receive any specific grant from funding agencies in the public, commercial, or not-for-profit sectors.

Declaration of Competing Interest

The authors declare that they have no known competing financial interests or personal relationships that could have appeared to influence the work reported in this paper.

Acknowledgments

The authors would like to thank EPFL colleagues Claude-Alain Jacot, Ioannis Mirtsopoulos, and Alex Muresan as well as students Prateek Kumar and Cornelius Carl for their dedicated help throughout manufacturing, assembly, exhibition, and documentation of the prototype pavilions. Financial support from Smart Living Lab, KUKA Switzerland, Debrunner, and Opitec for prototyping and manufacturing is thankfully acknowledged.

Appendix A. Supplementary Data

A video that shows the complete design and manufacturing process of the pavilion prototypes can be found online at https://doi.org/10.1016/j.autcon.2021.103614.

References

[1] J.M. Allwood, J.M. Cullen, Sustainable Materials: With both Eyes Open, UIT Cambridge, Cambridge, UK, 2012.
[2] S. Kaethner, J. Burridge, Embodied CO2 of structural frames, Struct. Eng. 90 (5) (2012) 33–40.

[3] International Energy Agency, Material efficiency in clean energy transitions, Paris. www.iea.org/publications/reports/MaterialEfficiencyinCleanEnergyTransitions, 2019. (Accessed 8 May 2019).
[4] E. Iacovidou, P. Purnell, Mining the physical infrastructure: opportunities, barriers and interventions in promoting structural components reuse, Sci. Total Environ. 557–558 (2016) 791–807, https://doi.org/10.1016/j.scitotenv.2016.03.098.
[5] M. Gorgolewski, Resource Salvation: The Architecture of Reuse, John Wiley & Sons, Hoboken, NJ, USA, 2017.
[6] J. Brütting, J. Desruelle, G. Senatore, C. Fivet, Design of Truss Structures through Reuse, Structures. 18 (2019) 128–137, https://doi.org/10.1016/j.istruc.2018.11.006.
[7] J. Brütting, C. Vandervaeren, G. Senatore, N. De Temmerman, C. Fivet, Environmental impact minimization of reticular structures made of reused and new elements through life cycle assessment and mixed-integer linear programming, Energy Build. 215 (2020) 109827, https://doi.org/10.1016/j.enbuild.2020.109827.
[8] C. Fivet, J. Brütting, Nothing is lost, nothing is created, everything is reused: structural design for a circular economy, Struct. Eng. 98 (1) (2020) 74–81.
[9] A.S. Howe, I. Ishii, T. Yoshida, Kit-of-parts - A review of object-oriented construction techniques, in: Proceedings of the ISARC'99 - International Symposium on Automation and Robotics in Construction, Madrid, 1999, pp. 165–171.
[10] S. Brancart, A. Paduart, A. Vergauwen, C. Vandervaeren, L. De Laet, N. De Temmerman, Transformable structures: Materialising design for change, Int. J. Des. Nat. Ecodyn. 12 (3) (2017) 357–366, https://doi.org/10.2495/DNE-V12-N3-357-366.
[11] L. Alegria Mira, A.P. Thrall, N. De Temmerman, Deployable scissor arch for transitional shelters, Autom. Constr. 43 (2014) 123–131, https://doi.org/10.1016/j.autcon.2014.03.014.
[12] M. Mengeringhausen, Raumfachwerke aus Stäben und Knoten: Theorie, Planung, Ausführung, 7th ed., Bauverlag, Wiesbaden, 1975.
[13] B. Guy, N. Ciarimboli, DfD: Design for Disassembly in the Built Environment: A Guide to Closed-Loop Design and Building, Hamer Center, 2008.
[14] N. De Temmerman, L. Alegria Mira, A. Vergauwen, Feasibility of the Universal Scissor Component (USC): building a full-scale deployable dome, J. Int. Assoc. Shell Spatial Struct. 53 (4) (2012) 227–236.
[15] LANIK, Structural turnkey solutions. http://www.lanik.com/en, 2018 (accessed March 28, 2020).
[16] H. Schober, Transparent Shells: Form, Topology, Structure, 1st ed., Ernst & Sohn, Berlin, Germany, 2015.
[17] A. Rochas, Universal Node for Space Frame Structures, US Patent US8820025B1, 2014, 17 March 2020.
[18] Hubs, hubs = geodesic domes made simple. https://buildwithhubs.co.uk/, 2020 (accessed March 28, 2020).
[19] I.M. de Oliveira, R.M. de O. Pauletti, L.C. Meneghetti, Connection system for gridshell structures using parametric modeling and digital fabrication, Autom. Constr. 109 (2020) 102996, https://doi.org/10.1016/j.autcon.2019.102996.
[20] P. Brescia, C. Calderini, B. Mongiardino, M. Pongiglione, T. Principi, A. Traverso, An innovative reusable modular system for steel truss structures, in: International Conference of the Architectural Science Association, The Architectural Science Association (ANZAScA), Australia, 2013, pp. 599–608.
[21] H. Pottmann, A. Asperl, M. Hofer, A. Kilian, Architectural Geometry, 1st edition, Bentley Institute Press, Exton, Pa, 2007.
[22] G. Austern, I.G. Capeluto, Y.J. Grobman, Rationalization methods in computer aided fabrication: a critical review, Autom. Constr. 90 (2018) 281–293, https://doi.org/10.1016/j.autcon.2017.12.027.
[23] A. Lobel, Lobel Frames. http://www.equilatere.net/, 1993. (Accessed 17 March 2020).
[24] A. Lobel, Formes et structures engendrées par des éléments identiques, A, Lobel, Bourg-la-Reine, 1993.
[25] C. Jiang, C. Tang, M. Tomičí, J. Wallner, H. Pottmann, Interactive modeling of architectural freeform structures: combining geometry with fabrication and statics, in: P. Block, J. Knippers, N.J. Mitra, W. Wang (Eds.), Advances in Architectural Geometry 2014, Springer International Publishing, Cham, 2015, pp. 95–108, https://doi.org/10.1007/978-3-319-11418-7_7.
[26] M. Huard, M. Eigensatz, P. Bompas, Planar panelization with extreme repetition, in: P. Block, J. Knippers, N.J. Mitra, W. Wang (Eds.), Advances in Architectural Geometry 2014, Springer International Publishing, Cham, 2014, pp. 259–279, https://doi.org/10.1007/978-3-319-11418-7_17.
[27] C.-W. Fu, C.-F. Lai, Y. He, D. Cohen-Or, K-set tilable surfaces, ACM Trans. Graph. 29 (4) (2010) 1–6, https://doi.org/10.1145/1778765.1778781.
[28] M. Singh, S. Schaefer, Triangle Surfaces with Discrete Equivalence Classes, in: ACM SIGGRAPH 2010 Papers, Association for Computing Machinery, Los Angeles, California, 2010, pp. 1–7, https://doi.org/10.1145/1833349.1778783.
[29] S. Lloyd, Least squares quantization in PCM, IEEE Trans. Inf. Theory 28 (2) (1982) 129–137, https://doi.org/10.1109/TIT.1982.1056489.
[30] P. Basso, A.E. Del Grosso, A. Pugnale, M. Sassone, Computational morphogenesis in architecture: cost optimization of free-form grid shells, J. Int. Assoc. Shell Spatial Struct. 50 (3) (2009) 143–150.
[31] F. Otto, J. Hennicke, IL10 Gitterschalen - Gridshells, Karl Krämer Verlag, Stuttgart, 1975.
[32] C. Douthe, R. Mesnil, H. Orts, O. Baverel, Isoradial meshes: covering elastic gridshells with planar facets, Autom. Constr. 83 (2017) 222–236, https://doi.org/10.1016/j.autcon.2017.08.015.
[33] A. Koronaki, P. Shepherd, M. Evernden, Rationalization of freeform space-frame structures: reducing variability in the joints, Int. J. Archit. Comput. 18 (1) (2020) 84–99, https://doi.org/10.1177/1478077119894881.
[34] H. Zimmer, F. Lafarge, P. Alliez, L. Kobbelt, Zometool shape approximation, Graph. Model. 76 (5) (2014) 390–401, https://doi.org/10.1016/j.gmod.2014.03.009.
[35] L. Alegria Mira, A.P. Thrall, N.D. Temmerman, The universal scissor component: optimization of a reconfigurable component for deployable scissor structures, Eng. Optim. 48 (2) (2016) 317–333, https://doi.org/10.1080/0305215X.2015.1011151.
[36] A. Tugilimana, A.P. Thrall, R. Filomeno Coelho, Conceptual design of modular bridges including layout optimization and component reusability, J. Bridg. Eng. 22 (11) (2017), https://doi.org/10.1061/(ASCE)BE.1943-5592.0001138.
[37] J. Brütting, G. Senatore, C. Fivet, Form follows availability - designing structures through reuse, J. Int. Assoc. Shell Spatial Struct. 60 (4) (2019) 257–265, https://doi.org/10.20898/j.iass.2019.202.033.
[38] McNeel & Associates, Rhino 6. https://www.rhino3d.com/, 2018 (accessed April 21, 2020).
[39] McNeel & Associates, Grasshopper - algorithmic modeling for Rhino. https://www.grasshopper3d.com/, 2018 (accessed April 21, 2020).
[40] D. Piker, Kangaroo3d, Kangaroo3d. http://kangaroo3d.com/, 2020. (Accessed 20 May 2020).
[41] A.S. Day, An introduction to dynamic relaxation, Engineer. 219 (1965) 218–221.
[42] M.R. Barnes, Form finding and analysis of tension structures by dynamic relaxation, Int. J. Space Struct. 14 (2) (1999) 89–104, https://doi.org/10.1260/0266351991494722.
[43] D. Piker, Kangaroo: form finding with computational physics, Archit. Des. 83 (2) (2013) 136–137, https://doi.org/10.1002/ad.1569.
[44] G. Senatore, D. Piker, Interactive real-time physics: an intuitive approach to form-finding and structural analysis for design and education, Comput. Aided Des. 61 (2015) 32–41, https://doi.org/10.1016/j.cad.2014.02.007.
[45] S. Bouaziz, S. Martin, T. Liu, L. Kavan, M. Pauly, Projective dynamics: fusing constraint projections for fast simulation, ACM Trans. Graph. 33 (4) (2014) 1–11, https://doi.org/10.1145/2601097.2601116.
[46] H. Wang, M. Song, Ckmeans.1d.dp: Optimal k-means Clustering in One Dimension by Dynamic Programming, R J. 3 (2) (2011) 29–33, https://doi.org/10.32614/RJ-2011-015.
[47] V. Volčini, viliwonka/Sharp-CKMeans. https://github.com/viliwonka/Sharp-CKMeans, 2020. (Accessed 14 April 2020).
[48] D. Piker, Dan-Piker/K2Goals. https://github.com/Dan-Piker/K2Goals, 2016. (Accessed 23 March 2020).
[49] D. Bertsimas, J.N. Tsitsiklis, Introduction to Linear Optimization, Athena Scientific, Belmont, Mass, 1997.
[50] L.L.C. Gurobi Optimization, Gurobi Optimizer Reference Manual. http://www.gurobi.com, 2019.
[51] The Math Works Inc, Matlab R2018a, The Math Works Inc., 2018. https://www.mathworks.com/products/matlab.html. (Accessed 14 April 2020).
[52] SOFiSTiK AG, Sofistik 2018 Finite Element Analysis. https://www.sofistik.com/, 2018. (Accessed 12 June 2020).
[53] M. Delorme, M. Iori, S. Martello, Bin packing and cutting stock problems: mathematical models and exact algorithms, Eur. J. Oper. Res. 255 (1) (2016) 1–20, https://doi.org/10.1016/j.ejor.2016.04.030.
[54] O. Salem, A. Shahin, Y. Khalifa, Minimizing cutting wastes of reinforcement steel bars using genetic algorithms and integer programming models, J. Constr. Eng. Manag. 133 (12) (2007) 982–992, https://doi.org/10.1061/(ASCE)0733-9364(2007)133:12(982).